(Received 24 February 2025, Accepted 29 September 2025, Scheduled 25 October 2025)

High Efficiency Low Power RF Energy Harvesting System for LTE Band and IoT Applications

Bilal Salman Taha[1,*], Zeti Akma Rhazali[1], Jahariah Binti Sampe[2], Norun Farihah Abdul Malek[3], Mohammed Yousif Zeain[4], and Adel M. Alkaseh[5,6]

[1]*Department of Electrical and Electronics Engineering, University Tenaga Nasional, Malaysia*
[2]*Institute of Microengineering and Nanoelectronics (IMEN), Universiti Kebangsaan Malaysia (UKM), Malaysia*
[3]*ECE Department, Kulliyyah of Engineering, International Islamic University Malaysia, Kuala Lumpur, Malaysia*
[4]*Centre for Telecommunication Research & Innovation (CeTRI)*
Faculty of Engineering and Technology Electronics and Computer (FTKEK)
Universiti Teknikal Malaysia Melaka (UTeM), Melaka 76100, Malaysia
[5]*Faculty of Industrial and Manufacturing Technology and Engineering, Universiti Teknikal Malaysia Melaka*
Hang Tuah Jaya, 76100 Durian Tunggal, Melaka, Malaysia
[6]*Polymer Research Centre, Tripoli, Libya*

ABSTRACT: The prospective applications of a rectangular microstrip patch antenna (MPA) in energy harvesting (EH) at radio frequencies were investigated. The study aims to develop a rectenna that can detect and connect low power wireless devices to long-term evolution (LTE) networks by capturing low-power radio frequency (RF) signals radiated by cell towers, since the Kappa 438 antenna substrate with relative permittivity 4.25 has high 9 dB gain and 83% of measured efficiency. For the 2.5 GHz LTE band, stubs technology was used for impedance matching and to decrease the overall rectenna size. The captured RF signals were altered into a usable DC voltage via a rectifier circuit in the manufactured rectenna, having the option of storing the voltage in a battery or utilizing it to power wearable, portable Internet of Things (IoT) systems and wireless sensors. The rectifier circuit is reduced in size by utilizing the SMD-Schottky diode type SMS7630 segments approach, further reducing the complexity and bulk of the rectenna. The rectenna obtained an efficiency of 88% when the RF input power is tuned to 0 dBm, while the maximum output DC voltage generated was 1.7 V when the radio waves power supply is 10 dBm. The rectenna with high gain and directivity has the capability to operate in low power environments, capturing weak radio frequency signals and working across −10 to 10 dBm power dynamic range. These outcomes represent new contribution to our work which is relevant to other studies listed in Table 6 and demonstrated notable improvements.

1. INTRODUCTION

The proliferation of low-power devices, such as sensors, computers, and communication instruments, has driven significant interest in sustainable power solutions, particularly for Internet of Things (IoT) applications. Traditional batteries pose substantial challenges, including the high cost and logistical complexity of replacement and maintenance [1–3]. Radio Frequency Energy Harvesting (RFEH) offers a compelling alternative by converting ambient electromagnetic waves from sources like cellular networks, Wi-Fi, and television broadcasts into a usable direct current (DC) voltage as shown in Fig. 1. This process enables the development of self-sufficient, battery-free sensors, which not only reduces costs but also minimizes maintenance efforts. Previous research has confirmed the feasibility of wireless power transfer, demonstrating that low-power devices can benefit from efficient RF-to-DC conversion [4–6].

Recent studies have explored diverse approaches to optimize RF energy harvesting systems. One notable development is a flexible rectenna array designed for omnidirectional harvesting, which uses a direct conjugate matching technique to eliminate the need for a traditional, lossy matching network [7].

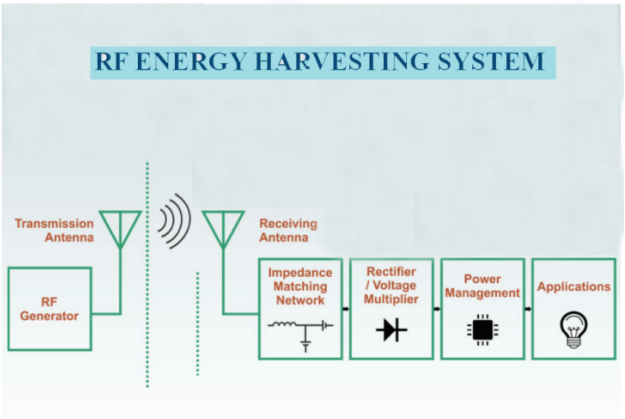

FIGURE 1. The graph of RF energy harvesting system.

This system operates at 2.45 GHz with a reported efficiency of 50%. Another compact, dual-band rectenna for 2.45 GHz and 5.8 GHz has been proposed, employing a complex impedance correlation matching technique to achieve efficiencies of 65.1% and 38.4%, respectively [8]. Furthermore, to address the challenge of high-power applications, a system was developed that

* Corresponding author: Bilal Salman Taha (belalsal@yahoo.com).

uses a radial power divider to distribute a 10 W RF input to multiple Schottky diodes, allowing them to operate at peak efficiency and deliver several watts of DC power [9]. Ref. [10] proposes a self-powered system for mobile phones using a stretchable multiband rectenna to harvest RF energy from multiple frequencies (900 MHz to 2.45 GHz). The system intelligently switches between communication and energy harvesting modes based on battery level, aiming to reduce charging needs by **60–90%** despite mechanical deformations. Building on these advancements, this study presents a high-efficiency rectenna system specifically designed for the 2.5 GHz Long-Term Evolution (LTE) band. A rectangular microstrip patch antenna (MPA) has been theoretically and experimentally designed using CST Microwave Studio (MWS)® to capture RF signals from various sources within this critical frequency range, including cellular towers, Wi-Fi, and WiMAX networks. The choice of the 2.5–2.7 GHz spectrum is particularly relevant given its role in expanded mobile broadband capacity. The successful development of an antenna capable of receiving RF signals from cell towers and converting them into usable energy demonstrates the practical feasibility of this approach for powering IoT devices within an LTE network.

Our proposed system employs a rectenna manufactured with an SMS7630 SMD-Schottky diode to minimize the size and complexity of the rectifier circuit, which is essential for resource-constrained IoT devices [11]. The stubs technique was also implemented as an optimization tool to further reduce the rectenna's dimensions and enhance its integration and performance [12]. The system's remarkable efficiency of 88% at a power input level of 0 dBm highlights its capability to convert low RF energy range from -10 to 10 dBm into a usable DC voltage, making it a strong candidate for energy harvesting applications [13]. The ability to store the harvested energy in a battery is a critical component that mitigates the unpredictability of RF signal supply, ensuring a consistent power source for devices [14].

2. ANTENNA DESIGN

The MPA's major advantages include its conformal printing capabilities, minimal weight, and planar design, which enable it to be directly printed on a Printed Circuit Board (PCB). Additionally, it is compact and has a low profile, and the essential characteristics of an MPA are illustrated [3, 15].

Figure 2 illustrates that a transmission line (TL) composed of a highly conductive metal, typically copper, is connected to a radiation array with dimensions L and W to provide MPA. The radiation patch and TL are located on top of the substrate, with the dielectric constant (ε_r) and height (h) indicated. The backdrop plane is situated below the substrate [16, 17].

This section develops, simulates, debates, and optimizes the antenna's critical design parameters and features to improve its properties, including gain, S_{11}, bandwidth (BW), and radiation pattern. The Antenna Magus application was employed to simplify the antenna design process in this investigation. In the appropriate sequence, the operating frequency, height, material type, relative permittivity of the Rogers substrate (ϵr), and input reactance of the antenna can be selected prior to antenna

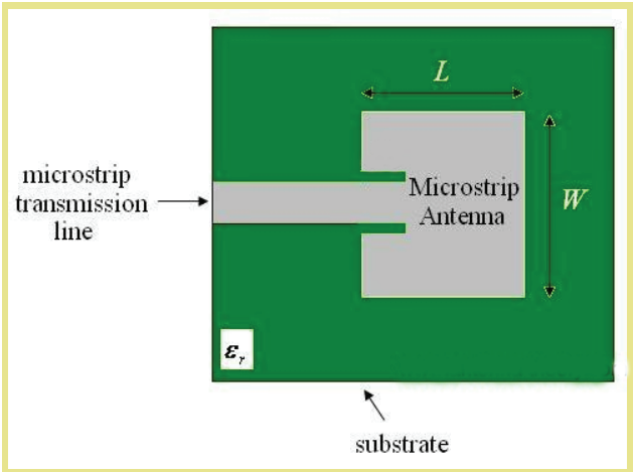

FIGURE 2. The rectangular microstrip patch antenna.

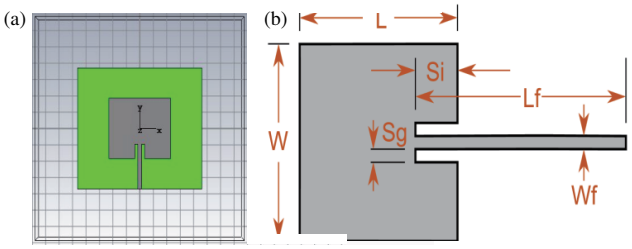

FIGURE 3. The patch antenna and its dimensions. (a) Patch Antenna using CST-MWS. (b) Patch and feed line dimensions.

TABLE 1. Essential parameters values.

Parameter List	Symbol	Dimension
Resonance Frequency	f_r	2.5 GHz
Dielectric Constant	ε_r	4.25
Height of Substrate	h	1.524 mm
Input Impedance	Z_{in}	50 Ω
Material Type	Rogers Kappa — 438	

design. Table 1 displays the parameters employed in this investigation, while Fig. 3 illustrates the patch antenna's dimensions within the Computer Simulation Technology Microwave Studio (CST-MWS).

After completing the antenna simulation in the Antenna Magus simulation software, the designed model is exported to CST-MWS software in order to apply the optimization procedure and export the Gerber file for manufacturing purposes. The optimization procedure is done by minimizing or maximizing some of the antenna's dimensions or other factors, like the substrate's thickness or relative permittivity and the desired gain. Through optimization, bandwidth, return loss, impedance matching, and the fabrication of antennas are all improved [4, 18]. Table 2 illustrates the parameter values obtained from Antenna Magus before and after the optimization procedure.

TABLE 2. The single MPA parameters values before and after optimization.

Parameter	Antenna Magus (mm)	Optimized Value (mm)
Patch Width (W)	35.779	36
Patch Length (L)	27.703	27
Feed inset inside the patch (S_i)	8.266	10
Feed line width (Wf)	2.917	3
Feed line length (Lf)	31.9	27
The gap between the feed line and patch (S_g)	3	0.55

Equations (1)–(5) are used for validating the results of the simulation from Antenna Magus [19];

$$\varepsilon_{reff} = \frac{\varepsilon_r + 1}{2} + \frac{\varepsilon_r - 1}{2}\left[1 + 12\frac{h}{w}\right]^{\frac{-1}{2}} \quad (1)$$

$$\Delta L = 0.412h\frac{(\varepsilon_{reff} + 0.3)\left[\frac{w}{h} + 0.264\right]}{(\varepsilon_{reff} - 0.258)\left[\frac{w}{h} + 0.8\right]} \quad (2)$$

$$L_{eff} = \frac{c}{2f_r\sqrt{\varepsilon_{reff}}} \quad (3)$$

$$L = L_{eff} - 2\Delta L \quad (4)$$

$$W = \frac{c}{2f_r\sqrt{\frac{(\varepsilon_r+1)}{2}}} \quad (5)$$

where ε_{reff} is the effective permittivity; L_{eff} is the effective length; and a distance is added to the patch's dimensions on each end to increase its length (ΔL). The patch antenna's ultimate configuration is the outcome of numerous optimization iterations, as illustrated in Fig. 4. The MPA may be fed using various methods, including aperture coupling, proximity coupling, inset feeding, and pin feeding [6, 11].

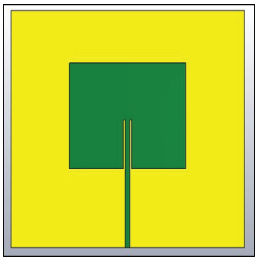

FIGURE 4. Optimized patch antenna with inset feed using CST-MWS (1).

The input reactance may be diminished if the patch is applied closer to the center, as the current at the end of a half-wave patch is significantly lower at the center [12, 16]. In the current study, the inset feeding approach is employed to simplify impedance matching, antenna fabrication, and rectifier circuit connection.

2.1. Simulation Results

After the antenna has been simulated and optimized via CST-Studio, this section presents the findings obtained from CST MWS transient solver.

2.1.1. Return Loss (S_{11})

Figure 5 illustrates the Return Loss (S_{11}) of simulated output of the optimized MPA at 2.5 GHz. A -40 dB of S_{11} was acquired whereas the voltage standing wave ratio (VSWR) was calculated and equal to 1.01, as shown in the following equation [20]:

$$\text{VSWR} = \frac{(10^{(\frac{S11}{20})} + 1)}{(10^{(\frac{S11}{20})} - 1)} \quad (6)$$

2.1.2. Bandwidth

Based on the S_{11} graph, the antenna's bandwidth can be determined. The lowest bandwidth of the antenna could be accepted when S_{11} is less than -9.5 dB. The -10 dB of S_{11} is approximately equal to 2 of VSWR, so it is the lowest acceptable case [21, 22]. Fig. 6 illustrates the bandwidth of the rectangular MPA (RMPA), which is calculated to be equal to 35.147 MHz at the center frequency of 2.5 GHz (around 1.4%).

2.1.3. Radiation Pattern and Gain

Poor gain is one of the most known drawbacks of the MPA. This is because the substrate thickness and relative dielectric constant have an impact on the antenna's gain, which has a direct relationship with substrate thickness and an inverse relationship with εr [23, 24]. The achieved gain and 3D radiation pattern in this work are equal to 6.94 dB, as demonstrated in Figs. 7(a), (b) which shows a 2D plot of the radiation pattern. A single main lobe with a medium beamwidth dominates a patch's radiation pattern. It illustrates the 3 dB beamwidth for the patch antenna after optimization, which is about 91°.

2.1.4. Antenna Radiation Efficiency

The ability of an antenna refers to its ability to transform electrical power into emitted electromagnetic power. This important antenna performance indicator shows the percentage of input power that is truly emitted as electromagnetic waves [25]. While a lower efficiency suggests that more power is wasted within the antenna or reflected because of impedance mismatch, a greater efficiency means more of the given power is radiated, as illustrated in Fig. 8.

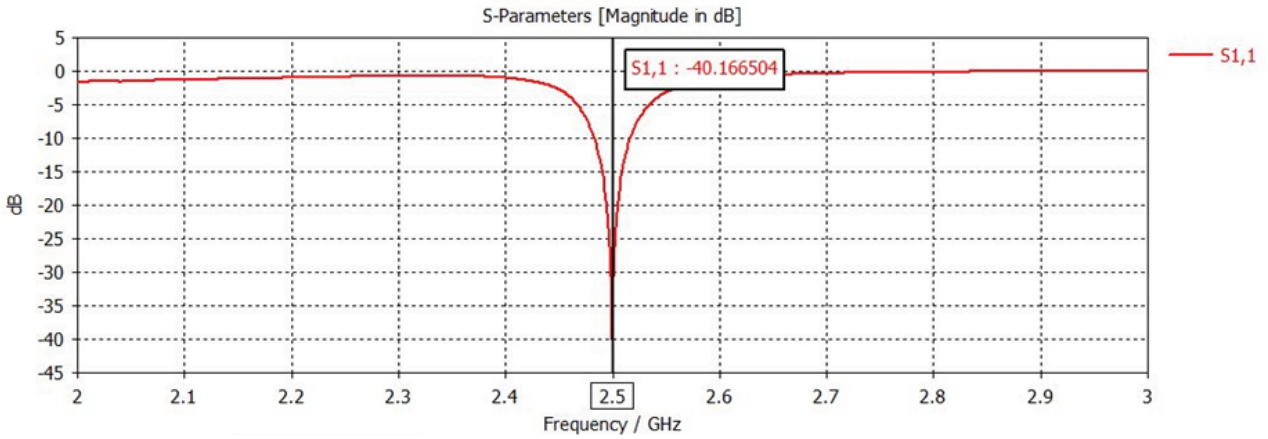

FIGURE 5. The S_{11} of the optimized MPA at 2.5 GHz.

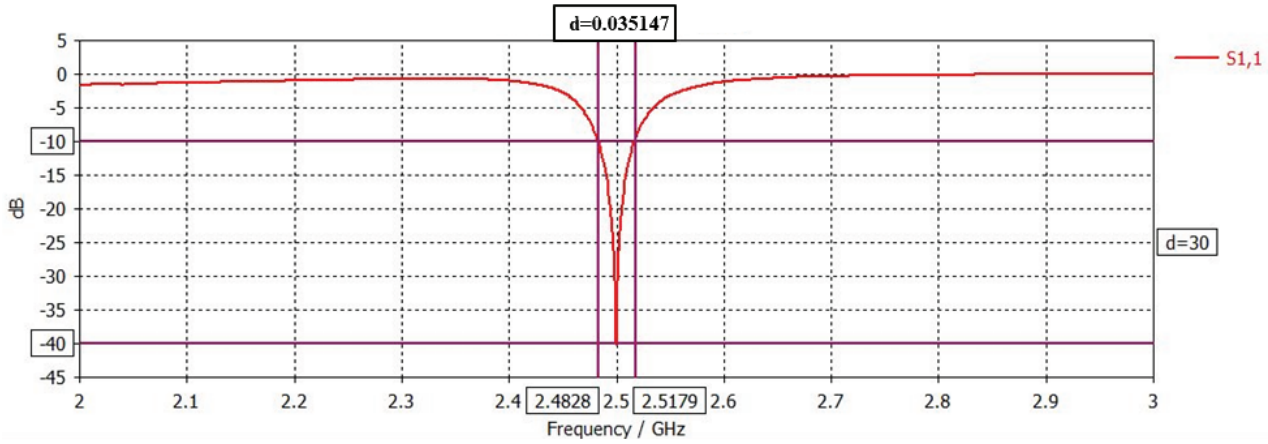

FIGURE 6. Bandwidth of the simulated antenna.

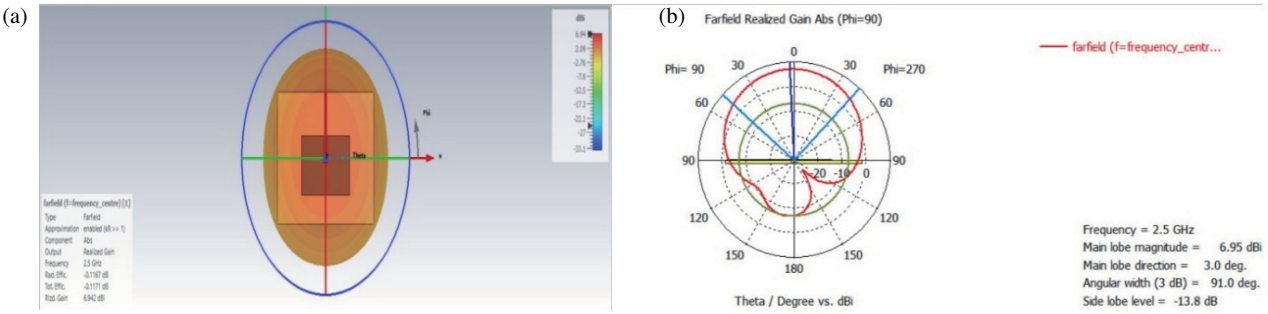

FIGURE 7. Simulated MPA gain. (a) 3D, (b) 2D radiation pattern.

The antenna efficiency can be determined, by dividing the radiated power by incident antenna power, as shown in Equation (7) below [26],

$$Ae = \frac{Pr}{Pi}\%, \tag{7}$$

where,

Ae: The antenna efficiency (%).

Pr: The radiated power from antenna.

Pi: The input power to the antenna.

From Fig. 8, the antenna accepted power is 0.49 W, while the antenna radiated power is to 0.47 W, so the antenna efficiency will be equal to: $Ae = (0.48/0.49) * 100 = 97.95\%$.

2.2. Manufacturing and Calculating Process

The antenna manufacturing and calculation process are discussed and investigated in this section.

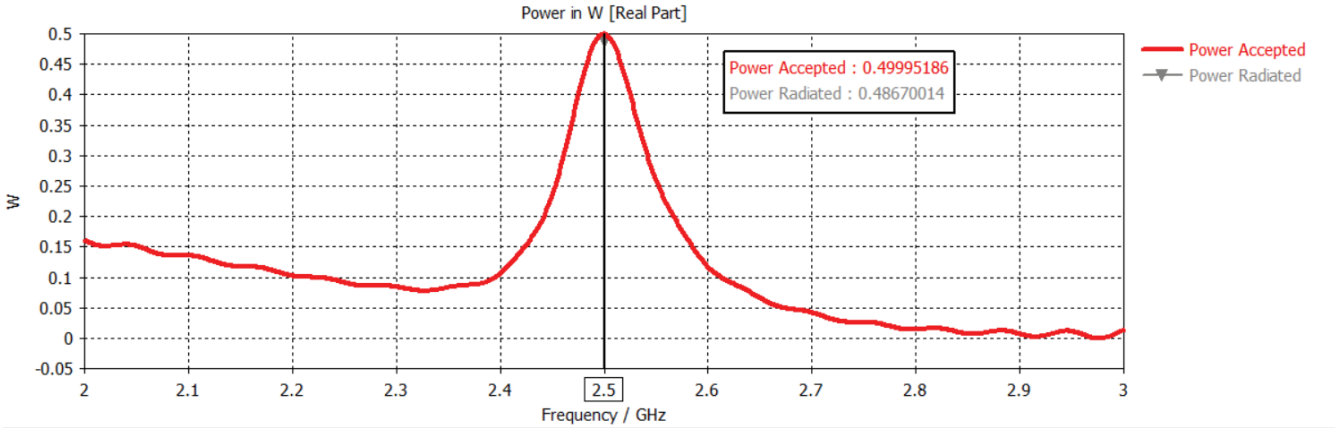

FIGURE 8. Simulated antenna efficiency.

TABLE 3. Received power and gain calculations.

Parameter	Value
Received reference antenna power	−34 dBm
AUT received power	−36 dBm
Reference antenna gain	11 dBi
The received power — reference received power	2 dB
The AUT gain	11 dBi − 2 dB = 9 dBi

2.2.1. Antenna Fabrication

Following the completion of the antenna simulation process, the antenna manufacturing process starts by exporting the Gerber file structure from CST-MWS and sending it to the factory. Fig. 9 illustrates the manufactured antenna under test (AUT).

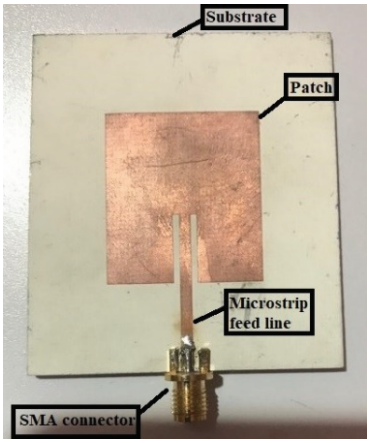

FIGURE 9. The fabricated antenna under test (AUT) at 2.5 GHz.

In this work, the Anritsu S362E Site Master Antenna Analyser is used to measure the S_{11} and VSWR, as depicted in Figs. 10–11, respectively.

By comparing Figs. 5 and 10, it can be observed that the S_{11} of simulated and fabricated antennas at 2.5 GHz of the resonance frequency are in good agreement. Fig. 12 demonstrates the analysis of the simulated and measured return losses of the AUT at 2.5 GHz. Three steps are taken to utilize real-world data of the received power, antenna radiation pattern, and gain at the resonant frequency of 2.5 GHz. First, a Proxicast Yagi 11 dBi high-gain 3G/4G/LTE Wi-Fi directional Yagi antenna (700–2700) MHz was used as a reference antenna. It was installed and aligned inside an anechoic chamber room to prepare for the testing process, as illustrated in Fig. 13.

Second, the function generator was set at 2.5 GHz resonant frequency with 0 dBm transmitted power, as illustrated in Fig. 14. The received reference antenna power is then recorded in Table 3. Finally, the received reference antenna was replaced with the manufactured AUT, as illustrated in Fig. 15. The calculation of the antenna received power and gain is recorded in Table 4.

The AUT's far-field radiation pattern was practically measured by changing the direction of the antenna for several degrees and recording the received power in each case [27]. The antenna beamwidth equal to 90° was obtained from the demonstrated measurements in Table 4 while Fig. 16 shows the measured far-field radiation pattern.

From Figure 16, the fabricated antenna efficiency can be calculated through the following equation:

$$\text{Directiviy } (D) = \frac{41000}{\theta\text{HPBW} * \Phi\text{HPBW}} \tag{8}$$

The values of θ and Φ could be obtained from Figure 16 at (−3 dB) of half-power bandwidth (HPBW) which is equal to 60°, yielding the directivity as follows:

$$\text{Directiviy } (D) = \frac{41000}{(60°) * (60°)} = 11.38°.$$

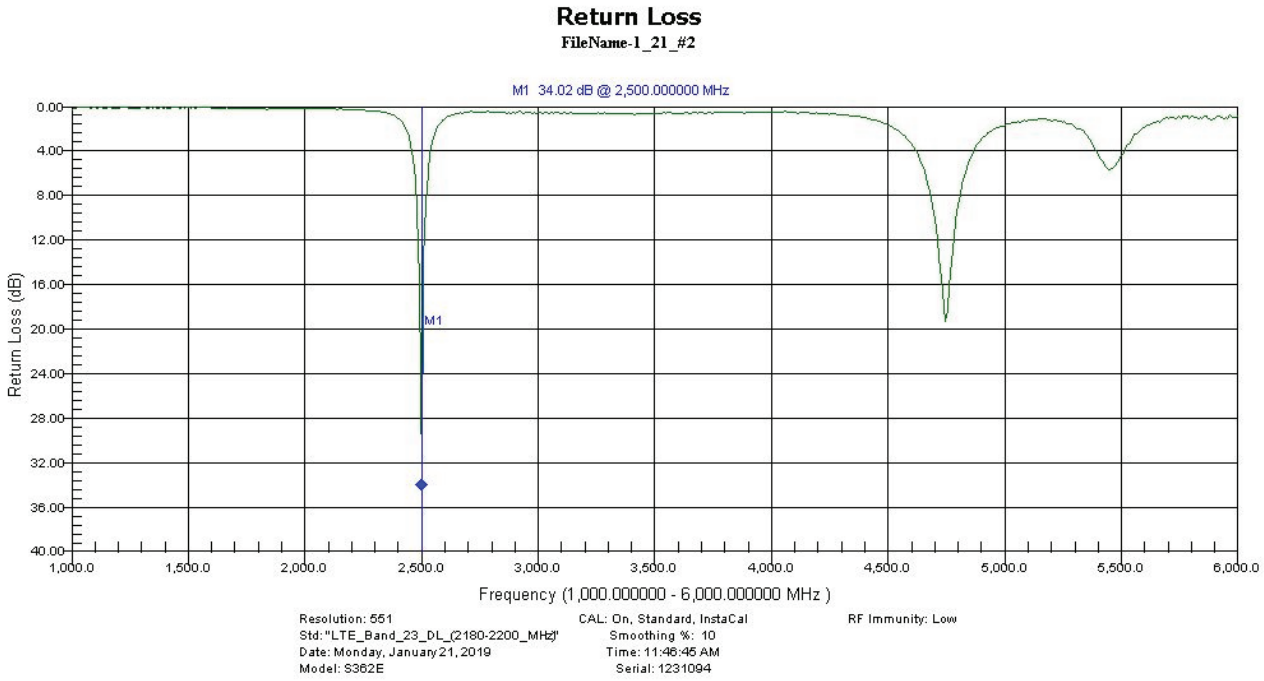

FIGURE 10. S_{11} of the AUT at 2.6 GHz.

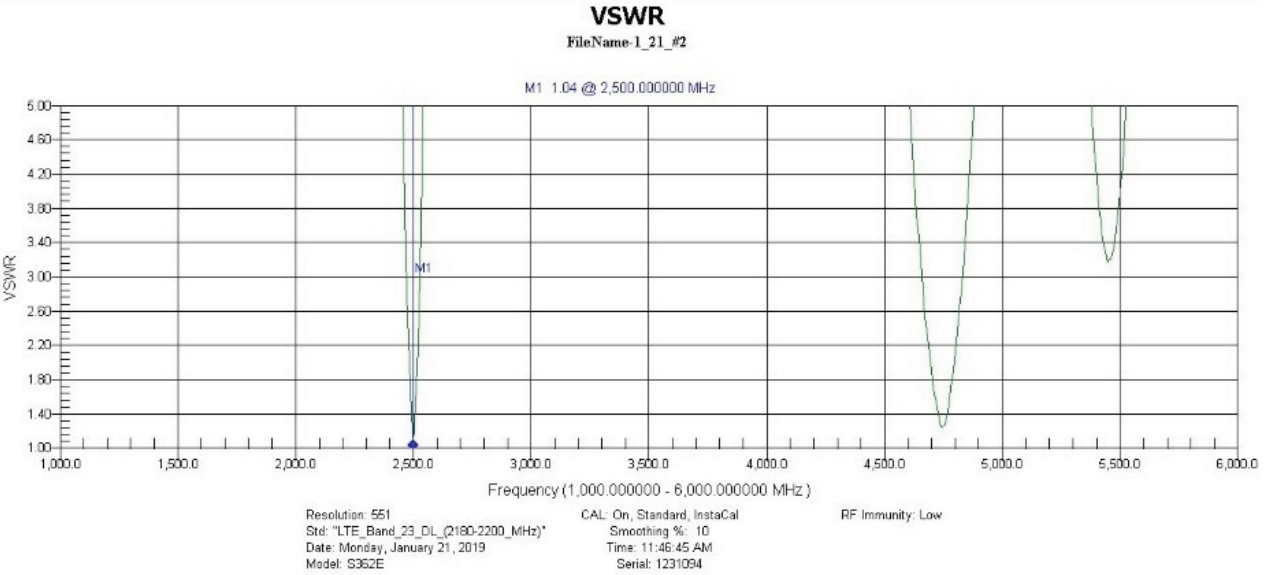

FIGURE 11. VSWR of the AUT at 2.5 GHz.

TABLE 4. Measured antenna radiation pattern.

Angle (Degree)	**0**	**45**	**90**	**130**	**180**	**220**	**270**	**310**	**350**	**360**
Received Power (dBm)	-36	-40	-75	-78	-80	-80	-76	-40	-36	-36

After that, the directivity value is converted from a ratio to decibels:

$$10\log(11.83) = 10.73\,\text{dB},$$

Finally, the fabricated antenna efficiency is calculated as:

$$Ae = \frac{\text{Gain}\,(G)}{\text{Directivity}\,(D)} = \frac{9\,\text{dB}}{10.73\,\text{dB}} = 0.838 * 100 = 83.87.$$

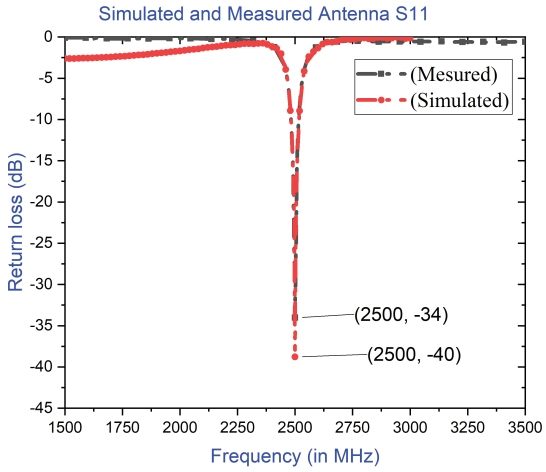

FIGURE 12. Comparison of simulated and measured S_{11} at 2.5 GHz.

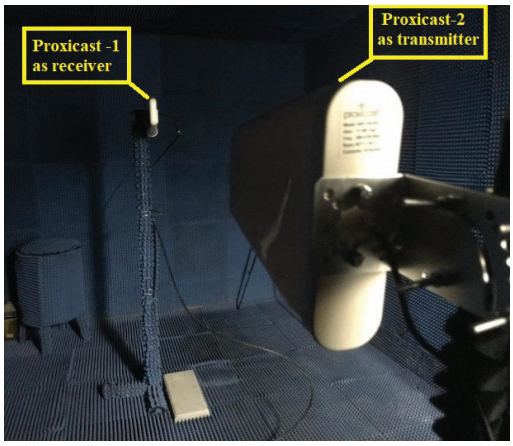

FIGURE 13. Alignment of 11 dBi Poxicast Yagi antenna in a chamber room.

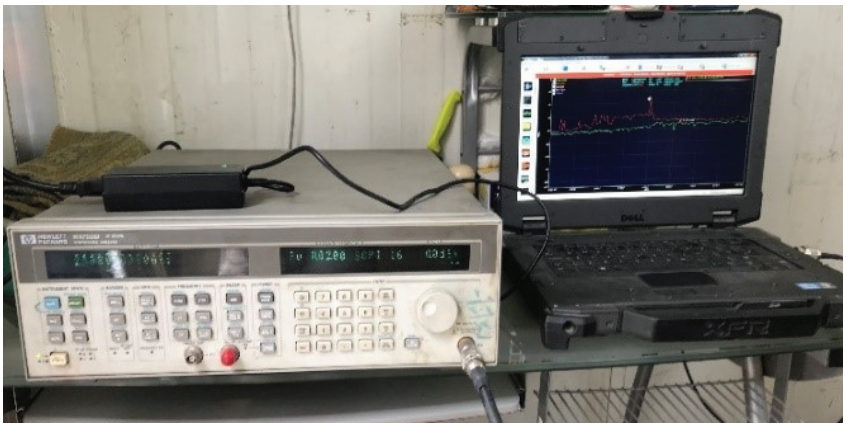

FIGURE 14. Setting of the function generator.

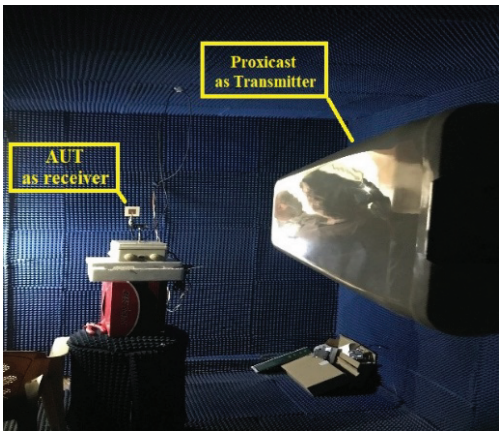

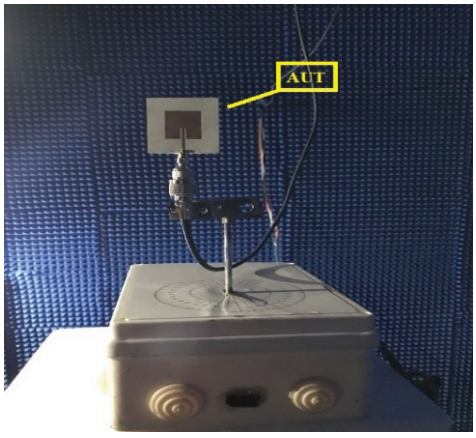

FIGURE 15. The manufactured AUT as receiver.

The manufactured antenna has a good and acceptable radiation efficiency value, which helps to increase the total rectenna efficiency by improving the sensitivity of the antenna and allowing the rectenna to work under low RF power environment.

3. RECTIFIER CIRCUIT DESIGN

A rectifier circuit in the harvesting antenna is a passive element working without any internal power feeding source or active elements that rectify the alternating wave received by the antenna. The voltage doubler rectifier circuit is a voltage multi-

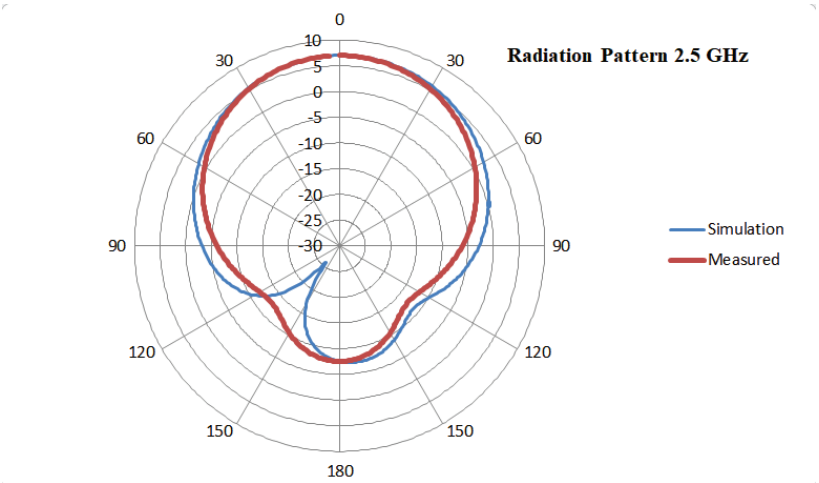

FIGURE 16. The far-field radiation at 2.5 GHz.

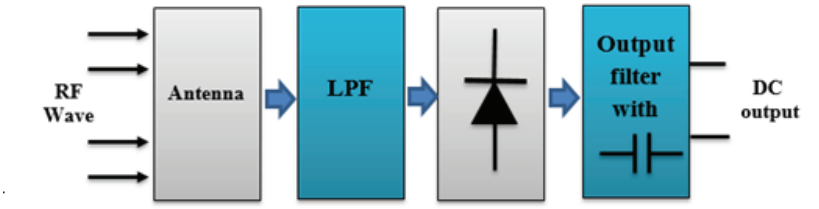

FIGURE 17. General block diagram of a rectenna circuit.

plier, which has a voltage multiplication factor of two. In other words, the output Direct Current (DC) level is equivalent to doubling the input DC level, and the voltage doubler's output directly feeds a low-power device. For the rectifier, a rectifier circuit was used to amplify the alternating current (AC) current received by the antenna from the free space. Nonlinear rectifying circuit components, such as diodes, could generate fundamental frequency harmonics [17, 30]. The rectenna efficiency is reduced due to unwanted harmonics and electromagnetic (EM) interference.

In an effort to mitigate the reradiation of higher harmonics by the nonlinear components, two stubs were implemented between the antenna and rectifier circuit, to work as impedance matching circuit (i.e., low-pass filter (LPF)). Utilizing a single-shunt rectifier along with an output filter for RF-DC conversion enhances conversion efficiency and stabilizes the DC voltage. A generic representation of the rectenna is depicted in Fig. 17 [18].

Voltage rectification and voltage multiplication from RF energy into DC energy were accomplished by the RF-DC rectifier, a fundamental component of the RFEH front-end circuit. Since the captured RF energy had a low power density, the power supplied to the rectifier had to be rectified and multiplied to provide sufficient DC power to the output load. The performance of the rectifier was assessed using the following factors:

1. **Rectifier Sensitivity**

   The sensitivity of a rectifier is the lowest amount of input power needed to produce a DC output load. It is a crucial indicator to make sure that the wireless energy harvesting (WEH) system is operational and capable of operating dependably in a real-world setting. The expression for the rectifier's sensitivity is provided by:

$$PdBm = 10 * \log_{10}(PmW) \tag{9}$$

   where PmW is the power received by the rectifier, expressed in milliwatts, and $PdBm$ is the rectifier's sensitivity, expressed in dBm.

2. **Power Conversion Efficiency (PCE)**

   The ratio of a rectifier's DC output power to its AC input power is known as its power conversion efficiency. Basically, it measures how well alternating current (AC) is converted to direct current (DC) by a rectifier. A higher efficiency means that less power is lost as heat or in other ways and that more input AC power is transformed into usable DC power, which is determined by the equation mentioned in (10).

3. **Power Dynamic Range (PDR)**

   The power dynamic range of a rectifier is the ratio between the highest and lowest input power levels at which the rectifier can function effectively. This range indicates how well a rectifier can manage different input power levels while still performing at the intended level with power conversion efficiency (PCE) commonly used as the evaluation metric [28]. Wider dynamic range is essential for applications like energy harvesting and wireless power transfer because it allows the rectifier to operate efficiently across a larger range of input power.

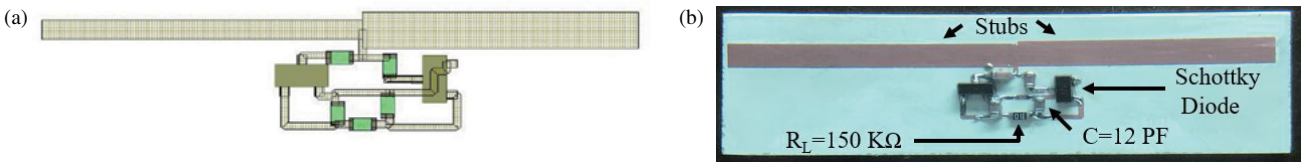

FIGURE 18. (a) The layout of the rectifier circuit. (b) The implemented rectifier circuit.

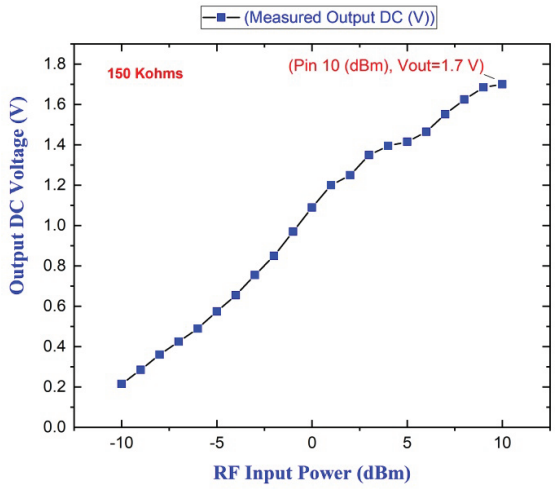

FIGURE 19. Rectifier output voltage related to input RF power.

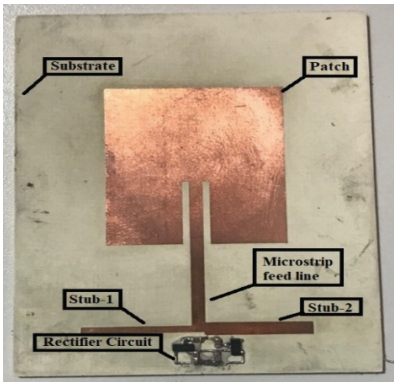

FIGURE 20. The integrated design of the rectenna.

3.1. Fabrication of Rectifier Circuit

First, the layout of the rectifier circuit is designed inside the Microwave Office®; Fig. 18 shows the simulated Greinacher voltage doubler rectifier circuit, which comprises two Schottky diodes, four capacitors, and load resistance (R_l). Schottky diode was chosen to reduce the voltage drop where its threshold is approximately equal to 0.15 V. This low threshold enables more effective operation at low incident power levels.

Also, to obtain a lower junction capacitance than PN diodes, the rectifier circuit is fabricated on a Roger Kappa-438 substrate, with 0201 SMD components mounted on the substrate to reduce the overall rectenna dimensions. The harmonic frequencies are suppressed using two stubs instead of a low-pass filter (LPF), ensuring that only the 2.5 GHz signal is allowed to pass. In the rectenna structure, the rectenna's highest power conversion efficiency (PCE) could be achieved through the cancellation of the corresponding matching circuit among the antenna and rectifier circuit [20, 28]. To further minimize the rectenna size and avoid the complexity of implementing an LPF as a matching circuit, stubs are employed. The first stub, 15 mm in length, is placed on the left side, while the second stub, 17 mm in length, is placed on the right. The stubs used should match the antenna's and rectifier's circuit impedance. Also, to minimize the rectenna size and complexity of implementing the LPF as a matching circuit. The coupling is a crucial matter to ensure the superior power transmission from the antenna to the rectifier circuit. A single stage Greinacher charge pump is used as to rectify the circuit, which converts the alternating electrical signal that is received by the antenna from the free space, then converts it to useful DC output voltage. Figs. 18(a), (b) illustrate the implemented rectifier circuit and fabricated design of the rectifier, respectively, while Fig. 20 illustrates the integrated design of the rectenna.

The experimental setup in the chamber room is prepared to evaluate the performance of the rectifier circuit coupled with the AUT (i.e., the rectenna), as shown in Fig. 21. An Hewlett-Packard (HP) 83752B Synthesized Sweeper 0.01–20 GHz function generator is employed to generate the 2.5 GHz resonance frequency with the required level of power. An HP 8595E spectrum analyzer is used to measure the S_{11}, and the output from R_L of the rectenna is found using a digital multimeter, Pro'skit MT-1232. To evaluate the rectifier performance, the function generator is set to different levels of transmitting power. The measured output voltage of the rectifier as a function to input power is illustrated in Fig. 19 for resistive load of 150 KOhms.

As observed in Fig. 19, the rectenna demonstrates sensitivity to low input power, enabling operation within a low RF input power range. In addition, the rectenna can operate effectively over a wider power dynamic range (-10 to 10 dBm). The maximum output voltage achieved is 1.7 V when the received RF_Power is 10 dBm.

FIGURE 21. DC output voltage measurement procedure.

TABLE 5. Power conversion efficiency calculation.

Transmitter Power (dBm)	Transmitter Power (mW)	Pin = Pac (mW) From Friis Formula	Pdc (mW)	Power Conversion Efficiency $\eta = \frac{Pdc}{Pac} \times 100\%$
-10	0.1	9.11×10^{-4}	3×10^{-4}	33
-9	0.125	1.139×10^{-3}	5.415×10^{-4}	47
-8	0.158	1.44×10^{-3}	8.64×10^{-4}	60
-7	0.2	1.8×10^{-3}	1.2×10^{-3}	66
-6	0.251	2.28×10^{-3}	1.6×10^{-3}	70
-5	0.316	2.88×10^{-3}	2.2×10^{-3}	76
-4	0.398	3.628×10^{-3}	2.94×10^{-3}	81
-3	0.5	4.5×10^{-3}	3.8×10^{-3}	84
-2	0.63	5.74×10^{-3}	4.81×10^{-3}	83
-1	0.794	7.23×10^{-3}	6.27×10^{-3}	86
0	1	9×10^{-3}	7.92×10^{-3}	88
1	1.25	0.0113	9.6×10^{-3}	85
2	1.58	0.014	0.011	78
3	2	0.018	0.012	66
4	2.5	0.022	0.0129	58
5	3.16	0.0288	0.0133	46
6	3.98	0.036	0.0143	39.7
7	5	0.045	0.016	35.5
8	6.3	0.057	0.018	31.5
9	7.94	0.072	0.0189	26
10	10	0.0911	0.02	22

For the rectenna power conversion efficiency, the following formula can be used [29];

$$\eta_r = \frac{P_{dc}}{P_{in}}, \tag{10}$$

where P_{dc} is the rectifier DC power which can be calculated from the rectifier output DC voltage measured with a meter divided by the resistive load (R_L). On the other hand, P_{in} which represents the power AC can also be calculated using the Friis transmission formula for free space path loss, as given in Equation (11).

$$P_{in} = \frac{P_t GtGr\lambda^2}{(4\pi r)^2}, \tag{11}$$

where P_t, G_t, G_r denote the transmission power, transmitter, and receiver antenna gain, respectively, while the rectifier output power P_{dc} can be calculated through the following equation:

$$P_{dc} = \frac{V_{DC}^2}{R_l}, \tag{12}$$

Figure 22 illustrate the rectenna power conversion efficiency_(PCE) as a function of input RF power. The rectenna achieves its highest efficiency of 88% at 0 dBm input power, while its lowest efficiency 33% occurs at -10 dBm, corresponding to 215 mV. The rectenna power efficiency changes due to the diode behavior at different levels of input power and the received RF power density. Table 5 provides the method to calculate the rectenna power conversion efficiency.

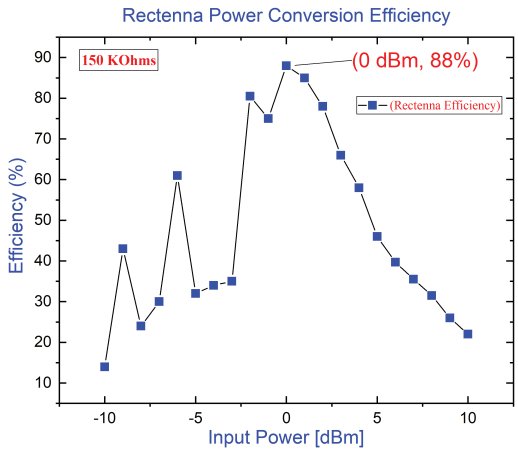

FIGURE 22. Rectenna power conversion efficiency (PCE)%.

The aim of this study is to recover energy from the LTE band. A compact rectenna was obtained with a positive gain and the highest PCE. The maximum output voltage is 1.7 V when the received power is 10 dBm and 1 meter away from the RF source. Table 6 provides an adaptable and useful option for the present wireless energy harvesting communication systems, especially in settings where space is limited, and effective energy harvesting is essential.

TABLE 6. Comparison of our effort with other studies.

Ref No.	Frequency (GHz)	Substrate	Antenna Type	Total Dimensions (mm × mm)	Gain (dB)	Output Voltage (V)	PCE (%)	Key Finding
[32]	0.55–2.5	FR4	Patch	160 × 160	2.5–5	400–600 mV for indoor & outdoor scenario	80	Lossy FR4 limits efficiency at high frequencies; low gain and low output DC voltage
[33]	1.73/2.47/2.53	FR4	Patch	48 × 48	(1.73, 2.47, 2.53) GHz are (3.8, 1.7 and 1.9) dBi Respectively	0.9	40% @ 2.53 GHz	Low efficiency, low gain antenna acceptable output voltage
[34]	0.79–0.96; 1.71–2.17; and 2.5–2.69	Paper	Copper Tape	11 × 11	1.3 dBi @900 MHz; 2.3 dBi @ 940 MHz; (4–6) dBi @ 2.5–2.69	1.02	Overall 57	Intermediate efficiency, acceptable output voltage, low gain antenna
[35]	2.4–2.5	Paper	Copper Tape	4.9 × 5.4	(−8 to 3) dBi	60 mV	28	Low efficiency, low output voltage and very low antenna gain
[36]	(1.85, 2.25, 2.6, 3.52, 5.01, and 5.89) GHz	F4B	Patch	NA	NA	0.25 @−10 dBm	41.33% @ 2.6 GHz	Low rectifier efficiency, low output voltage, the antenna gains not mentioned
[37]	(0.95, 2.1, 2.4, and 7) GHz	FR4	Patch	45 × 50	1–4	0.65, 0.85, 1.6 @ 30 dBm	50	Intermediate efficiency, very high input power, low antenna gain
[38]	1.8, 2.1, 2.4, and 2.6	FR4	Patch	120 × 130 × 1.525	7.5	1 @ 0 dBm	79.5% at 1.8 GHz	Good efficiency and output voltage with high antenna gain
[39]	2.5 to 25 GHz	RT4003	Patch	32 × 31 × 1.575 mm^3	7	250 mV	25	Low efficiency and output voltage, good antenna gain
[40]	2.37–2.70 GHz	RO3010	NA	19.75 × 15.20	NA	NA	66.25	Intermediate rectifier efficiency output voltage and antenna gain not mentioned
This work	**2.5**	**Rogers Kappa-438**	**Patch**	73 × 61.5	**9**	**1.7 @ 10 dBm and 1 @ 0 dBm**	**88 % @ 0 dBm**	The highest rectenna efficiency and high antenna gain with acceptable output voltage, indicating its potential application in the RF energy harvest

This work presents a rectenna design with significant advantages in power dynamic range, conversion efficiency, high output voltage under low-power conditions, and a high antenna gain. These contributions enable the rectenna to operate effectively across a wide range of wireless sensors and IoT applications, reducing dependence on external power sources.

4. FUTURE WORK

The research lays a solid foundation for future advancements. While the current architecture demonstrates high efficiency, future work should focus on optimizing the rectifier circuit and antenna materials for improved efficacy. It is also crucial to investigate the system's stability and endurance under diverse environmental conditions to ensure long-term, reliable performance. A key limitation of the current design is its single-frequency operation. Future efforts will therefore explore developing multiband rectennas to function in scenarios where the primary LTE band is unavailable.

Building on the successful application of the Grey Wolf Optimizer (GWO) algorithm for antenna design, future research will also explore advanced artificial intelligence (AI) methodologies to further enhance the gain and efficiency of novel rectenna structures [31]. This technology holds significant potential for leveraging ubiquitous RF energy from cellular networks to power wireless sensors in remote locations, paving the way for a more sustainable and interconnected future.

5. CONCLUSION

RF_EH technology is seen as a promising future technique for low-power devices, such as electrical and remote sensor appliances. In order to receive the low-radiated signal from the free space and transform it into an electrical signal that feeds the rectifier circuit, the proposed high gain MPA 9 dB design was examined. To put it another way, the antenna converts the electrical wave to the rectifier circuit after collecting the electromagnetic radio pattern at a 2.5 GHz LTE range. Antenna Magus and CST MWS were used to simulate the design. The Schottky diode model SMS-7630 was used to create the Greinacher voltage doubler rectifier circuit, which is a compact design and a major improvement over the Villard circuit for a tiny additional component cost. The main contributions of this work are the removal of the impedance matching (IM) lumped elements, lowering the overall dimensions of the rectenna, and the low rectenna sensitivity with a wider power dynamic rang (-10 to10) dBm. The rectifier's output voltage and conversion efficiency were examined. The indoor studies were carried out to assess the suggested rectenna's performance. Ultimately, the maximum output voltage of 1.7 V at 10 dBm is achieved, and the measured maximum efficiency is 88% at 1 mw (0 dBm) transmitted power.

REFERENCES

[1] Nintanavongsa, P., U. Muncuk, D. R. Lewis, and K. R. Chowdhury, "Design optimization and implementation for RF energy harvesting circuits," *IEEE Journal on Emerging and Selected Topics in Circuits and Systems*, Vol. 2, No. 1, 24–33, 2012.

[2] Taha, B. S., "Design of quad band microstrip patch antenna for electromagnetic energy harvesting applications," *Journal of Southwest Jiaotong University*, Vol. 54, No. 5, 1–9, 2019.

[3] Zbitou, J., M. Latrach, and S. Toutain, "Hybrid rectenna and monolithic integrated zero-bias microwave rectifier," *IEEE Transactions on Microwave Theory and Techniques*, Vol. 54, No. 1, 147–152, 2006.

[4] Taha, B. S. and H. M. Marhoon, "Simulation and manufacturing of modified circular monopole microstrip antenna for UWB applications," *International Journal of Advances in Applied Sciences (IJAAS)*, Vol. 10, No. 1, 70–78, 2021.

[5] Taha, B. S., H. M. Marhoon, and A. A. Naser, "Simulating of RF energy harvesting micro-strip patch antenna over 2.45 GHz," *International Journal of Engineering & Technology*, Vol. 7, No. 4, 5484–5488, 2018.

[6] Reddy, M. J. and D. N. Kumar, "Multi-objective particle swarm optimization for generating optimal trade-offs in reservoir operation," *Hydrological Processes: An International Journal*, Vol. 21, No. 21, 2897–2909, 2007.

[7] Fan, R., J. Mi, J. Jing, L. Yan, and C. Liu, "Conformal flexible omnidirectional rectenna array designed for application in iot smart water meters," *Progress In Electromagnetics Research C*, Vol. 139, 159–166, 2024.

[8] Li, L., R. Xu, J. Cao, X. Li, and J. Nan, "A compact loop-shaped dual-band omnidirectional rectenna for RF energy harvesting," *Progress In Electromagnetics Research M*, Vol. 125, 1–9, 2024.

[9] Kim, D. H., S. Y. Oh, H. S. Park, and S. K. Hong, "A power dividing rectenna system for high-power wireless power transfer for 2.45-GHz band," *IEEE Access*, Vol. 12, 86 631–86 638, 2024.

[10] Kar, P. C. and M. A. Islam, "Design and performance analysis of a rectenna system for charging a mobile phone from ambient EM waves," *Heliyon*, Vol. 9, No. 3, e13964, 2023.

[11] Sidibé, A., "Compact RF wireless power transmission system for battery-free geolocation tags," Ph.D. dissertation, University of Toulouse, Toulouse, France, 2023.

[12] Farooq, W., M. Ur-Rehman, Q. H. Abbasi, K. Q. Maqbool, and K. Qaraqe, "Study of a microstrip patch antenna with multiple circular slots for portable devices," in *2015 IEEE 8th GCC Conference & Exhibition*, 1–4, Muscat, Oman, 2015.

[13] Choi, K. W., A. A. Aziz, D. Setiawan, N. M. Tran, L. Ginting, and D. I. Kim, "Distributed wireless power transfer system for Internet of Things devices," *IEEE Internet of Things Journal*, Vol. 5, No. 4, 2657–2671, 2018.

[14] Arinze, S. N., E. R. Obi, S. H. Ebenuwa, and A. O. Nwajana, "RF energy-harvesting techniques: Applications, recent developments, challenges, and future opportunities," *Telecom*, Vol. 6, No. 3, 45, 2025.

[15] Thakur, E., D. Kumar, N. Jaglan, S. D. Gupta, and S. Srivastava, "Mathematical analysis of commonly used feeding techniques in rectangular microstrip patch antenna," in *Advances in Signal Processing and Communication: Select Proceedings of ICSC 2018*, 27–35, 2018.

[16] Muhamad, N. F., R. A. M. Osman, M. S. Idris, F. Jamlos, and N. A. M. A. Hambali, "Microwave and electrical properties of SrTiO3 for DRA application," *International Journal of Nanoelectronic Materials*, Vol. 11, No. 21, 231–236, 2018.

[17] Shinohara, N., "Rectennas for microwave power transmission," *IEICE Electronics Express*, Vol. 10, No. 21, 20 132 009–20 132 009, 2013.

[18] Rastogi, A. K., G. Pravin, and S. Sharma, "Comparative study of rectangular and E-shaped microstrip patch antenna array for X-band applications," in *Advanced Computing and Communication Technologies: Proceedings of the 11th ICACCT 2018*, 195–203,

Jul. 2018.

[19] Zeain, M. Y., M. Abu, A. A. Althuwayb, H. Alsariera, A. J. A. Al-Gburi, A. A. Abdulbari, and Z. Zakaria, "A new technique of FSS-based novel chair-shaped compact MIMO antenna to enhance the gain for sub-6 GHz 5G applications," *IEEE Access*, Vol. 12, 49 489–49 507, 2024.

[20] Taha, B. and T. AlSharabati, "Performance comparison between the FR4 substrate and the Rogers Kappa-438 substrate for microstrip patch antennas," *International Journal of Computer Science and Mobile Computing*, Vol. 9, No. 2, 1–12, 2020.

[21] Wang, Y., J. Zhang, Y. Su, X. Jiang, C. Zhang, L. Wang, and Q. Cheng, "Efficiency enhanced seven-band omnidirectional rectenna for RF energy harvesting," *IEEE Transactions on Antennas and Propagation*, Vol. 70, No. 9, 8473–8484, 2022.

[22] Zeain, M. Y., Z. Zakaria, M. Abu, A. J. A. Al-Gburi, H. Alsariera, A. Toding, S. Alani, M. A. Al-Tarifi, O. S. Al-Heety, H. Lago, *et al.*, "Design of helical antenna for next generation wireless communication," *Przegląd Elektrotechniczny*, Vol. 11, 96–99, 2020.

[23] Mishra, R. G., J. Jayasinghe, G. Chathuranga, and R. Mishra, "Analysis of the relationship between substrate properties and patch dimensions in rectangular-shaped microstrip antennas. intelligent communication, control and devices," in *Proceedings of ICICCD 2017*, Vol. 624, Springer Nature Link, Jan. 2018.

[24] Toding, A., N. Allu, M. Y. Zeain, and A. Lukas, "Investigation performance minimum mse relay design for MIMO multi-relay networks," *Solid State Technology*, Vol. 63, No. 6, 15 831–15 837, 2020.

[25] Zeain, M. Y., M. Abu, and S. N. Zabri, "Investigation of printed helical antenna using varied materials for ultra-wide band frequency," *Journal of Telecommunication, Electronic and Computer Engineering (JTEC)*, Vol. 10, No. 2–7, 137–142, 2018.

[26] Lou, X. and G.-M. Yang, "A dual linearly polarized rectenna using defected ground structure for wireless power transmission," *IEEE Microwave and Wireless Components Letters*, Vol. 28, No. 9, 828–830, 2018.

[27] Zeain, M. Y., M. Abu, Z. Zakaria, A. J. A. Al-Gburi, R. Syahputri, A. Toding, and S. Sriyanto, "Design of a wideband strip helical antenna for 5G applications," *Bulletin of Electrical Engineering and Informatics*, Vol. 9, No. 5, 1958–1963, Oct. 2020.

[28] Ibrahim, H. H., M. J. Singh, S. S. Al-Bawri, S. K. Ibrahim, M. T. Islam, A. Alzamil, and M. S. Islam, "Radio frequency energy harvesting technologies: A comprehensive review on designing, methodologies, and potential applications," *Sensors*, Vol. 22, No. 11, 4144, 2022.

[29] Kotani, K., T. Komiyama, Y. Chonan, and H. Yamaguchi, "Simple equation-based rectifier model and its application to efficient energy harvesting from amplitude modulation broadcasting radio waves," *IEEE Transactions on Microwave Theory and Techniques*, Vol. 73, No. 6, 3376–3387, Jun. 2025.

[30] Abdulbari, A. A., S. K. Abdul Rahim, P. J. Soh, M. H. Dahri, A. A. Eteng, and M. Y. Zeain, "A review of hybrid couplers: State-of-the-art, applications, design issues and challenges," *International Journal of Numerical Modelling: Electronic Networks, Devices and Fields*, Vol. 34, No. 5, e2919, 2021.

[31] Zeain, M. Y., M. Abu, A. Toding, Z. Zakaria, H. Alsariera, I. Ullah, A. A. Abdulbari, H. Yon, B. S. Taha, and M. I. Abbasi, "Advanced helical antenna design for X-band applications using AI," *Progress In Electromagnetics Research C*, Vol. 153, 201–211, 2025.

[32] Song, C., Y. Huang, P. Carter, J. Zhou, S. Yuan, Q. Xu, and M. Kod, "A novel six-band dual CP rectenna using improved impedance matching technique for ambient RF energy harvesting," *IEEE Transactions on Antennas and Propagation*, Vol. 64, No. 7, 3160–3171, 2016.

[33] Wang, M., L. Yang, and Y. Shi, "A dual-port microstrip rectenna for wireless energy harvest at LTE band," *AEU — International Journal of Electronics and Communications*, Vol. 126, 153451, 2020.

[34] Palazzi, V., J. Hester, J. Bito, F. Alimenti, C. Kalialakis, A. Collado, P. Mezzanotte, A. Georgiadis, L. Roselli, and M. M. Tentzeris, "A novel ultra-lightweight multiband rectenna on paper for RF energy harvesting in the next generation LTE bands," *IEEE Transactions on Microwave Theory and Techniques*, Vol. 66, No. 1, 366–379, 2018.

[35] Palazzi, V., C. Kalialakis, F. Alimenti, P. Mezzanotte, L. Roselli, A. Collado, and A. Georgiadis, "Performance analysis of a ultra-compact low-power rectenna in paper substrate for RF energy harvesting," in *2017 IEEE Topical Conference on Wireless Sensors and Sensor Networks (WiSNet)*, 65–68, Phoenix, AZ, USA, 2017.

[36] Sun, S., Y. Wang, B. Li, H. Xue, C. Zhang, F. Xu, and C. Song, "Dual-port six-band rectenna with enhanced power conversion efficiency at ultra-low input power," *Sensors*, Vol. 24, No. 23, 7433, 2024.

[37] Elshaekh, D. N., H. A. Mohamed, L. Y. A. E. Menam, K. A. Sharshar, and S. I. Kayed, "Multiband printed rectenna for radio frequency energy harvesting (RF-EH)," *Discover Electronics*, Vol. 2, No. 1, 39, 2025.

[38] Eltresy, N. A., O. M. Dardeer, A. Al-Habal, E. Elhariri, A. H. Hassan, A. Khattab, D. N. Elsheakh, S. A. Taie, H. Mostafa, H. A. Elsadek, and E. A. Abdallah, "RF energy harvesting IoT system for museum ambience control with deep learning," *Sensors*, Vol. 19, No. 20, 4465, Oct. 2019.

[39] Kayed, S. I., D. N. Elsheakh, H. A. Mohamed, and H. A. Shawkey, "Multiband microstrip rectenna using ZnO-based planar schottky diode for RF energy harvesting applications," *Micromachines*, Vol. 14, No. 5, 1006, May 2023.

[40] Muhammad, S., J. J. Tiang, and S. Bujang, "RF rectifier design for efficient WPT in medical implants: A wideband approach for white space WiFi and LTE applications," in *2024 IEEE Asia-Pacific Conference on Applied Electromagnetics (APACE)*, 347–350, Langkawi, Kedah, Malaysia, Feb. 2024.